Oral presentation | Multi-phase flow
Multi-phase flow-III
Mon. Jul 15, 2024 4:30 PM - 6:30 PM Room D

[3-D-02] A monolithic model of solid–liquid phase change problem

*HUI YAO[1], Mejdi Azaiez[1] （1. Bordeaux University, Bordeaux INP, I2M UMR 5295, 33400 Talence, France）

Keywords: phase field method, heat resistance, enhance phase change material, solid-liquid phase change, finite element method

Twelfth International Conference on Computational Fluid Dynamics (ICCFD12), Kobe, Japan, July 14-19, 2024

ICCFD12-2024-xxxx

A monolithic model of solid–liquid phase change problem

Hui Yao*,[1] and Mejdi Azaiez[1]
* Corresponding author: hui.yao@u-bordeaux.fr
[1]Bordeaux University, Bordeaux INP, I2M UMR 5295, 33400 Talence, France.

1 Abstract

Base on a solid-liquid phase change model on the phase field method, this talk gives two extended models in certain cases, one with added enhanced materials in the phase change material [1], one with convection phenomena [2].

1.1 Phase change problem with enhancers

In latent heat storage, certain non phase change materials (non-PCMs) with high thermal conductivity are incorporated into the phase change materials (PCMs) with the aim of enhancing the efficiency of heat/cold storage. We term this type of non-PCMs as 'enhancer', for example graphite and copper foam, usually with a complex skeleton structure [3, 4]. A phase field model describes the solidification and melting phenomena of PCMs with enhancers. This model is governed by the energy equation coupled with the Allen-Cahn equation. A penalty technique is applied in the Allen-Cahn equation to describe the complex structure of the non-PCMs. We use the concept of thermal resistance to define the boundary condition on the contact interface of two materials to ensure the temperature jump. Thanks to the hybrid dual formulation, the temperature can be solved as a monolithic function while satisfying the temperature jump on the material interface. The Raviant-Thomas (RT0) and P0 finite elements are used to solve the temperature, to satisfy the temperature jump on the interface. Simulations are performed using the open source finite element software `FreeFem++`. To improve computational efficiency, under the framework of `FreeFem++`, the mesh refinement is conducted by the `Mmg` module, and the parallelization is performed by the domain decomposition library `ffddm`. 2D and 3D simulations are carried out for both melting and solidification processes of a fossil-based organic PCM, CRODATHERM60 in the graphite skeleton on different porous structures to validate this model.

1.2 Phase change problem with natural convection

Numerical simulations of convective solid-liquid phase change problems have long been a complex problem due to the movement of the solid-liquid interface layer, which leads to a free boundary problem. The seond part of this talk introduces a convective phase change heat transfer model based on the phase field method. The governing equations consist of the incompressible Navier-Stokes-Boussinesq equations, the heat transfer equation, and the Allen-Cahn equation. The Navier-Stokes equations are penalised for imposing zero velocity within the solid region. For numerical methods, the mini finite element approach (`P1b-P1`) is used to solve the momentum equation spatially, the temperature and the phase field are approximated by the `P1b` elements. In the temporal discretization, the phase field and the temperature are decoupled from the momentum equation by using the finite difference method, forming a solvable linear system. A maximum bound principle for the phase field is derived, coming with an estimation of the tolerance of the time step size, which depends on the temperature range. This estimation guides the time step choice in the simulation. The accuracy and effectiveness of the proposed method have been validated through real-world cases of melting and solidification with linear or nonlinear buyangcy force, respectively. The simulation results are in agreement with experiments in references.

2 Governing equations

We list the three models for phase change problem: the classical model and two extended models based on the classical one.

2.1 Classical phase change model on phase change problem

The following phase change model has been introduced in 1992 [5]. According to the asymptotic analysis, solutions to the phase field equations formally approach those of a sharp interface model, the Stefan problem, which incorporates surface tension. The uniqueness and existence of the solution of the Stefan problem had been established in [6]. Let Ω be a bounded domain, $\partial\Omega = \Gamma_D \bigcup \Gamma_N$ is the boundary.
Model A (phase change model for pure PCM):

$$\begin{aligned}
&\alpha\varepsilon^2\phi_t = \varepsilon^2\Delta\phi - f(\phi) + \lambda\varepsilon(T - T_m)g(\phi), && \text{in } \Omega,\\
&\rho(\phi)c_p(\phi)T_t = \nabla\cdot(\kappa(\phi)\nabla T) - \frac{1}{2}\rho_s\Delta H_m\phi_t, && \text{in } \Omega,\\
&T = T_D,\ \partial_{\boldsymbol{n}}\phi = 0, && \text{on } \Gamma_D,\\
&\partial_{\boldsymbol{n}}T = 0,\ \partial_{\boldsymbol{n}}\phi = 0, && \text{on } \Gamma_N,\\
&T(\boldsymbol{x},0) = T_0,\quad \phi(\boldsymbol{x},0) = \phi_0, && \text{in } \Omega,
\end{aligned}$$

with

$$F(\phi) = \frac{1}{8}(\phi^2-1)^2, \qquad f(\phi) = F'(\phi) = \frac{1}{2}\phi(\phi^2-1),$$
$$G(\phi) = \frac{1}{5}\phi^5 - \frac{2}{3}\phi^3 + \phi, \quad g(\phi) = G'(\phi) = (1-\phi^2)^2.$$
$$\rho(\phi) = \frac{1-\phi}{2}\rho_s + \frac{1+\phi}{2}\rho_l, \quad c_p(\phi) = \frac{1-\phi}{2}c_{ps} + \frac{1+\phi}{2}c_{pl}, \quad \kappa(\phi) = \frac{1-\phi}{2}\kappa_s + \frac{1+\phi}{2}\kappa_l.$$

Here, the phase field function ϕ labels the solid phase as -1 and the liquid phase as 1. Between the two phases, there is a smooth transition of certain thickness ε. α is the thermal diffusivity of the PCM. $F(\phi)$ is the double-well potential. $G(\phi)$ ensures that the phase change temperature is active only at the interface, and has minimum at ±1. f and g are their corresponding derivatives so that $f(\pm1) = g(\pm1) = 0$. T represents the temperature. T_m is the melting temperature, T_D is the heating/cooling temperature on the boundary. ρ, c_p, and κ are the density, the specific heat capacity, and the thermal conductivity, respectively. ΔH_m is the latent heat per mass.

2.2 PCM with enhancers

A bounded domain Ω is considered in this case, includeing several circular enhancers inside (see an example given in Figure 1). The subdomain consisting of enhancers is denoted by $\Omega_B = \bigcup_{i=1}^{m}\Omega_{B_i}$, m is the number of enhancers. The PCM is filled up in $\Omega\backslash\Omega_B$, and the non-PCM in Ω_B. The definition of ϕ in $\Omega\backslash\Omega_B$ is as same as in model A, while the value of ϕ in Ω_B is fixed as:

$$\phi(\boldsymbol{x},t) = \begin{cases} 1, & \text{fluid}\\ -1, & \text{solid}\end{cases} \text{ in } \Omega\backslash\Omega_B, \quad \phi(\boldsymbol{x},t) = \begin{cases} 1, & \text{melting}\\ -1, & \text{solidification}\end{cases} \text{ in } \Omega_B. \tag{2}$$

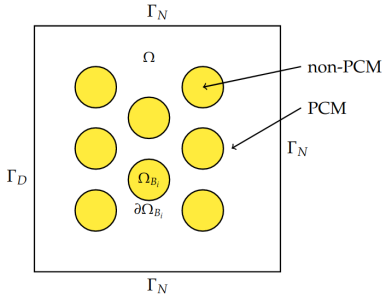

Figure 1: Domain with several enhancers.

As with the above definitions, within enhancers, our approach depends on the specific phase transition process: If the PCM in $\Omega\backslash\Omega_B$ transitions from the solid phase to the liquid phase (melting process), we set $\phi = 1$ to mark the non-PCM in Ω_B. Conversely, we set $\phi = -1$ if the PCM transitions from the liquid phase to the solid phase (solidification process). By distinguishing the labelling values of non-PCM during melting and solidification, in the initial state of phase field, we label the PCM and non-PCM by different values, this introduces a high-energy initial state, which ensures that the phase field always transits from high energy to low energy. This design ensures that the phase field model accurately reflects the energy evolution trend during the entire phase change process.

Taking account for the enhancers, we introduce a piece-wised characteristic function χ to indicate the position of enhancers, as follows:

$$\chi = \begin{cases} 0, & \boldsymbol{x} \in \Omega\backslash\Omega_B, \\ 1, & \boldsymbol{x} \in \Omega_B. \end{cases}$$

Let M be a constant larger than ε^{-2}. The model considering enhancers is given as follows:
Model B (phase change model for PCM with enhancers):

$$\begin{aligned}
&\alpha\varepsilon^2\phi_t = \varepsilon^2\Delta\phi - f(\phi) + \lambda\varepsilon(T - T_m)g(\phi) + \chi M(1 \pm \phi), && \text{in } \Omega, \\
&\rho(\phi)c_p(\phi)T_t = \nabla\cdot(\kappa(\phi)\nabla T) - \frac{1}{2}\rho_s\Delta H_m\phi_t, && \text{in } \Omega_B \bigcup (\Omega\backslash\Omega_B), \\
&[\kappa\partial_{\boldsymbol{n}}T] = 0,\ R(\kappa\partial_{\boldsymbol{n}}T) = [T], && \text{on } \partial\Omega_B, \\
&T = T_D,\ \partial_{\boldsymbol{n}}\phi = 0, && \text{on } \Gamma_D, \\
&\partial_{\boldsymbol{n}}T = 0,\ \partial_{\boldsymbol{n}}\phi = 0, && \text{on } \Gamma_N, \\
&T(\boldsymbol{x}, 0) = T_0, \quad \phi(\boldsymbol{x}, 0) = \phi_0, && \text{in } \Omega.
\end{aligned}$$

Density, heat capacity and conductivity are global functions of phase field ϕ and χ:

$$\begin{aligned}
\rho(\phi) &= (\frac{1-\phi}{2}\rho_s + \frac{1+\phi}{2}\rho_l)(1-\chi) + \rho_B\chi, \\
c_p(\phi) &= (\frac{1-\phi}{2}c_{ps} + \frac{1+\phi}{2}c_{pl})(1-\chi) + c_{pB}\chi, \\
\kappa(\phi) &= (\frac{1-\phi}{2}\kappa_s + \frac{1+\phi}{2}\kappa_l)(1-\chi) + \kappa_B\chi.
\end{aligned}$$

2.3 Phase change model with natural convection

A solid-liquid system is placed in a bounded domain Ω, governed by the incompressible Navier-Stokes equations, with the Boussinesq approximation accounting for buoyancy effects, and the phase change problem as in Model A. The velocity $\boldsymbol{u}$, the pressure p, the phase field ϕ and temperature T are solved by the following equations:
Model C (phase change model with convection):

$$\boldsymbol{u}_t + \boldsymbol{u}\cdot\nabla\boldsymbol{u} - \nu\Delta\boldsymbol{u} + \nabla p - A(\phi)\boldsymbol{u} = \mathbf{F_B}, \quad \text{in } \Omega, \tag{4a}$$

$$\nabla\cdot\boldsymbol{u} = \mathbf{0}, \quad \text{in } \Omega, \tag{4b}$$

$$\alpha\varepsilon^2\phi_t = \varepsilon^2\Delta\phi - f(\phi) + \lambda\varepsilon(T - T_m)g(\phi), \quad \text{in } \Omega, \tag{4c}$$

$$\rho c_p(T_t + \boldsymbol{u}\cdot\nabla T) = \nabla\cdot(\kappa\nabla T) - \frac{\rho_s\Delta H_m}{2}g(\phi)\phi_t, \quad \text{in } \Omega, \tag{4d}$$

$$T = T_D,\ \partial_{\boldsymbol{n}}\phi = 0, \boldsymbol{u} = \mathbf{0}, \quad \text{on } \Gamma_D, \tag{4e}$$

$$\partial_{\boldsymbol{n}}T = 0,\ \partial_{\boldsymbol{n}}\phi = 0, \boldsymbol{u} = \mathbf{0}, \quad \text{on } \Gamma_N, \tag{4f}$$

$$T(\boldsymbol{x}, 0) = T_0, \quad \phi(\boldsymbol{x}, 0) = \phi_0, \quad \text{in } \Omega. \tag{4g}$$

where ν is the dynamic viscosity of the PCM in fluid state. the Carman-Kozeny penalty term $A(\phi)\boldsymbol{u}$ ensures velocity vanishes in the solid region, and L denotes the liquid fraction within $[0, 1]$, as follows:

$$A(\phi) = -\frac{C_{CK}(1 - L(\phi))^2}{(L(\phi))^3 + b}, \quad L(\phi) = \phi\cdot(\phi > 0), \tag{5}$$

where $C_{CK} > 0$ is a sufficiently large number and $b > 0$ is a small number, to prevent the denominator from being zero. The buoyancy force $\mathbf{F}_B$ is linearized according to the Boussinesq approximation, reflecting the influence of temperature-induced density changes on the fluid dynamics:

$$\mathbf{F}_B = \frac{\rho(T) - \rho(T_m)}{\rho(T_m)} \boldsymbol{g} \approx \mathbf{e}_d \beta (T - T_m), \tag{6}$$

where $\boldsymbol{g}$ is the gravity, $\mathbf{e}_d$ is the unit vector in the vertical direction, and β is the thermal expansion coefficient.

3 Snippets of Simulation

We present one of our simulations in melting processes. Further details on our work are referred to our recent publication [1, 2].

3.1 Results for Model B

The 500×700 pixel binary image in the left of Figure 2 displays the porous medium structure obtained from a scanning electron microscope (ref. [7]). The domain size in this structure is 0.035×0.045 m^2, the white part represents the graphite skeleton, the black part represents CRODATHERM60. We perform the melting simulation. The left boundary acts as the heating boundary, with the remaining boundaries set as adiabatic. The initial mesh in the right of Figure 2 is refined on the skeleton outline and the left border.

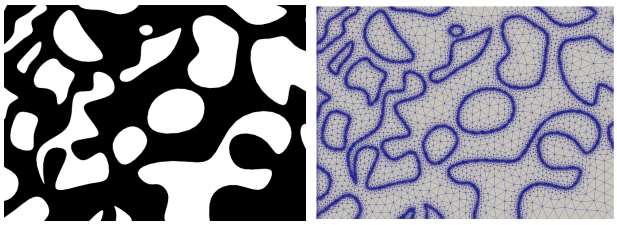

Figure 2: Porous media illustration: binary image (left), initial mesh (right).

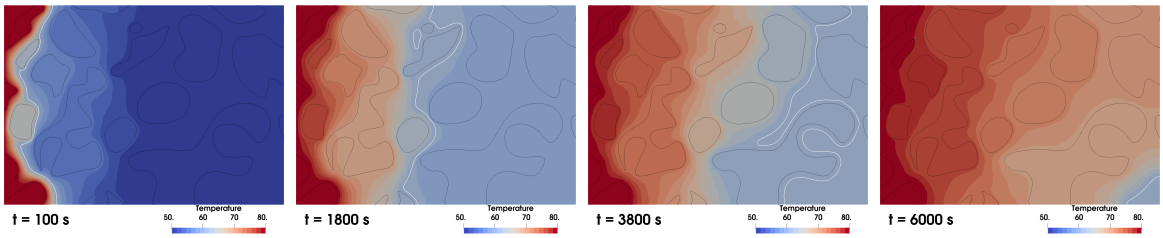

(a) Temperature contours

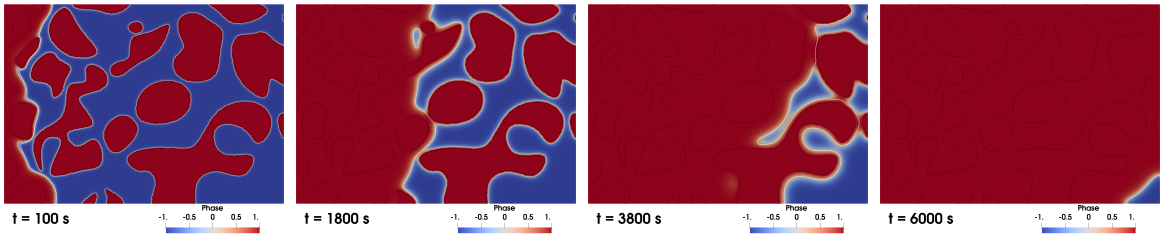

(b) Phase field contours

Figure 3: Porous media: temperature and phase field contours at $t = 100, 1800, 3800, 6000$ s.

Figure 3 shows the temperature and phase field contours at $t = 100, 1800, 3800, 6000$ s. The skeleton of graphite is always marked with $\phi = 1$, shown in red colour. Black lines outline the skeleton, and white

lines are the contours of $T = T_m$, coinciding with the interface of the phase field. It can be observed from Figure 3(a) that each piece of the skeleton is isothermal, implying that the heat transfer within the graphite piece is almost instantaneous.

3.2 Results for Model C

Model C is validated by a water freezing process, over temperatures from 10°C to −10°C, from an experiment of Kowalewski and Rebow in 1999 [8]. The nonlinear density variation of pure water below $T < 10.2°C$ leads to a nonlinear Boussinesq force. The density-temperature correlation is proposed by Gebhart and Mollendorf [9] as follows:

$$\rho(T) = \rho_f(1 - w|T - T_m|^q),$$

with the density $\rho_f = 999.972\,\mathrm{kg/m^3}$ on phase change temperature $T_m = 0°\mathrm{C}$, $w = 9.2793\times10^{-6}\,[(°\mathrm{C})^{-q}]$, with $q = 1.894816$. The temperature is mapping from the interval $[-10, 10]$ to $[-1, 1]$. Thus the scaled buoyancy force in (6) is expressed as:

$$\mathbf{F_B}(T) = \beta\omega|T|^q\boldsymbol{e}_d,$$

where $\beta = 5.21383 \times 10^8$ is the thermal expansion coefficient [10]. The dimensionless thermal conductivities for water are $\kappa_s = 3.91$ for solid and $\kappa_l = 1$ for liquid. To avoid nonlinearity of the energy equation, the global thermal conductivity is approximated as a linear combination of the previous phase field ϕ^n as follows:

$$\kappa(\phi^n) = \frac{1-\phi^n}{2}\kappa_s + \frac{1+\phi^n}{2}\kappa_l.$$

The computational domain is a unit square. The initial temperature is set at 0.5, above the melting temperature:

$$\boldsymbol{u}_0 = 0, \quad T_0 = 0.5, \quad \phi_0 = 1.$$

The boundary conditions are organized as follows:

$$\begin{aligned}
&\boldsymbol{u} = 0 \text{ on } \partial\Omega,\\
&T = 1 \text{ on } \Gamma_{hot}, T = -1 \text{ on } \Gamma_{cold},\\
&\phi = 1 \text{ on } \Gamma_{hot}, \phi = -1 \text{ on } \Gamma_{cold},\\
&\frac{\partial T}{\partial \boldsymbol{n}} = 0, \frac{\partial \phi}{\partial \boldsymbol{n}} = 0, \text{ on } \Gamma_{up} \cup \Gamma_{bottom}.
\end{aligned}$$

The other parameters are set as: $\varepsilon = 0.01, \alpha = 130, \lambda = 820, \rho = 1, c_p = 1, \Delta H_m = 8, \nu = 1, C_{ck} = 10^6, b = 10^{-7}, t_{\max} = 1.61$ and $h \in [0.002, 0.07]$. Time step size is set as $\Delta t = 0.001$.

In Figure 4(a), the final pressure distribution is depicted. The left portion of the figure, i.e. the liquid state, shows pressure values ranging from -3.2×10^4 to 3.1×10^4. The right portion corresponds to the solid state, wherein pressure values approximately equal to 0. Figure 4(b) displays an experimental image from Kowalewski and Rebow 1999 [8], with two vortices on the left liquid portion. The phase change temperature contours at $t = 0.75$ and $t = 1.61$ of our simulation are depicted, comparing with the simulation results of Sadaka [10]. Our contours match them well.

Figure 5 depicts the contours of the phase field, streamlines, and temperature at $t = 0.2, 0.6, 0.9$, and 1.61. In Figure 5(a), The streamlines show a non-uniform flow direction within the cavity, two vortices are formed. At $t = 1.61$, the streamlines resemble the experiment result in Figure 4(b). In Figure 5, the highest and lowest temperatures still occur at the top and bottom respectively, due to convection dominance. However, the temperature is not uniformly stratified because of the nonlinear buoyancy force. In summary, the model can well capture the flow patterns and phase transition dynamics, and reflect the nonlinear buoyancy effects.

References

[1] H. Yao and M. Azaiez. A monolithic model of solid–liquid phase change problem. *Comput. Methods Appl. Mech. Engrg.*, 421:116973, 2024.

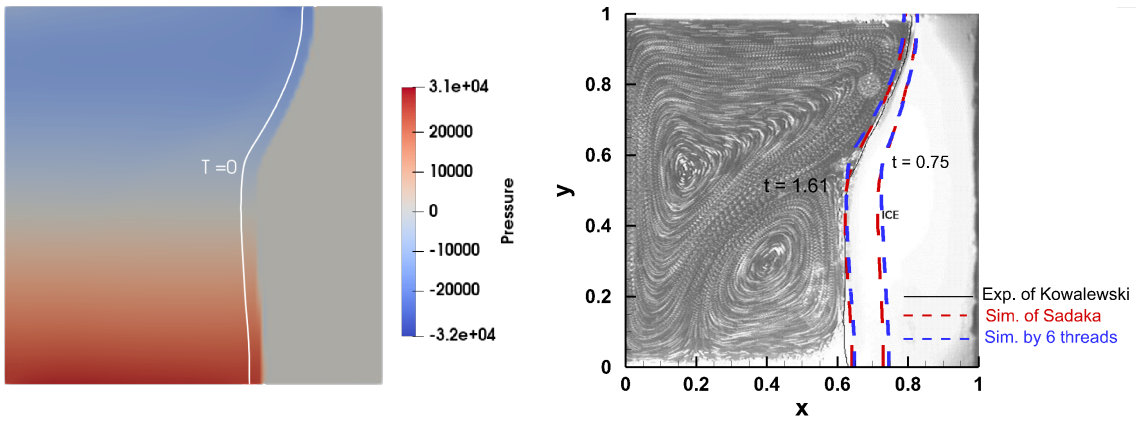

(a) (b)

Figure 4: Water freezing: (a) Pressure distribution at $t = 1.61$. (b) Comparison of interface positions: image from the experiment by Kowalewski and Rebow 1999 [8], our numerical results with 6 MPI processors, and numerical results from Sadaka et al. 2020 [10] at $t = 0.75$ and 1.61.

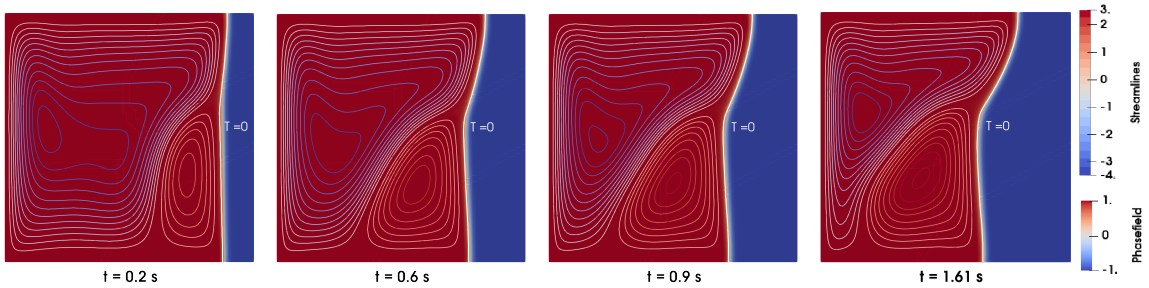

(a) Phaes field and streamlines contours.

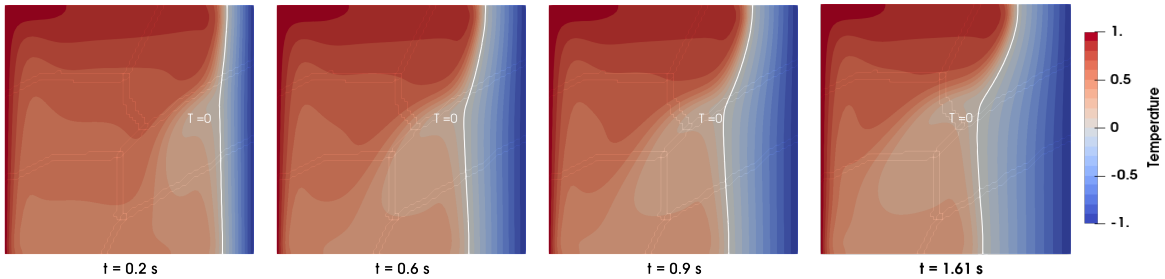

(b) Temperature contours.

Figure 5: Water freezing: phase field, streamlines and temperature contours at $t = 0.2, 0.6, 0.9$ and 1.61. The white line indicates the contour of the phase change temperature $T = 0$.

[2] H. Yao. A phase field method for convective phase change problem preserving maximum bound principle. *Appl. Numer. Math.*, 204:232–248, 2024.

[3] X.B. He, W. Wang, J. Qiu, Y.C. Hou, and Y. Shuai. Controllable preparation method and thermal properties of composite phase change materials based on starch pore formation. *Sol. Energy Mater Sol. Cells .*, 253:112255, 2023.

[4] X.H. Yang, Q.S. Bai, Q.L. Zhang, W.J. Hu, L.W. Jin, and J.Y. Yan. Thermal and economic analysis of charging and discharging characteristics of composite phase change materials for cold storage. *Appl. Energy*, 225:585–599, 2018.

[5] G. Caginalp and X.F. Chen. *Phase field equations in the singular limit of sharp interface problems.* Springer, 1992.

[6] X.F. Chen and F. Reitich. Local existence and uniqueness of solutions of the stefan problem with surface tension and kinetic undercooling. *J. Math. Anal. and Appl.*, 164:350–362, 1992.

[7] S. Sirivithayapakorn and A.A. Keller. Transport of colloids in saturated porous media: A pore-scale observation of the size exclusion effect and colloid acceleration. *Water Resour. Res.*, 39(4):1109, 2003.

[8] T. A. Kowalewski and M. Rebow. Freezing of water in a differentially heated cubic cavity. *Int. J. Comput. Fluid Dyn.*, 11(3-4):193–210, 1999.

[9] B. Gebhart and J. C. Mollendorf. A new density relation for pure and saline water. *Deep Sea Res.*, 24(9):831–848, 1977.

[10] G. Sadaka, A. Rakotondrandisa, P.-H. Tournier, F. Luddens, C. Lothodé, and I. Danaila. Parallel finite-element codes for the simulation of two-dimensional and three-dimensional solid–liquid phase-change systems with natural convection. *Comput. Phys. Commun.*, 257:107492, 2020.